J 14.4 MODELING ENTRAINMENT AND BOUNDARY LAYER GROWTH DURING A BORE EVENT USING DIFFERENT TURBULENCE PARAMETERIZATIONS AND LES

Mariusz Pagowski *
Cooperative Institute for Research in the Atmosphere/Forecast Systems Laboratory,
Colorado State University/NOAA

Steven E. Koch
NOAA Research - Forecast Systems Laboratory

J.-W. Bao
NOAA Research - Environmental Technology Laboratory

1. INTRODUCTION

The International H_2O Project (IHOP) field experiment took place in the Southern Great Plains of the U.S. with the goal of obtaining an improved characterization of the time varying three dimensional water vapor field and to determine its importance in the understanding and prediction of convective processes. Understanding the role played by bores in initiating and maintaining nocturnal convection was one of the objectives of the project.

Ground-based remote sensing instruments at the Homestead site in the Oklahoma Panhandle included NCAR Integrated Sounding System and Multiple Antenna Profiler (ISS/MAPR), an Atmospheric Emitted Radiance Interferometer (AERI), FM-CW radar, Scanning Raman Lidar and aerosol backscatter lidar (HARLIE). These instruments were complemented by the polarimetric S-POL and Dodge City WSR-88D radars and two research aircrafts equipped with the water vapor differential absorption lidar and surface mesonetwork recording temperature, dewpoint and wind at 5-min intervals.

The data gathered during IHOP constitutes probably the most comprehensive set of observations ever collected on structure and dynamics of bores. On 4 June 2002, two bores were observed at Homestead. Here, we analyze the ``second" bore which developed in the early morning on this day as a result of an interaction of a cold front with a stable boundary layer. This bore was well documented by the IHOP measurements. Numerical simulations with MM5 reproduced the event quite accurately and are used to study turbulence and boundary layer growth in the wake of the bore.

Our research will continue in the future using the Center for Analysis and Prediction of Storms (CAPS) ARPS model (Xue et al. 1995) at resolutions of the order of tens of meters with the purpose of evaluating turbulence parameterizations vs. simulations with explicitly resolved eddies.

* Dr. Mariusz Pagowski, email: Mariusz.Pagowski@noaa.gov

2. BACKGROUND AND METEOROLOGY

An internal bore is a gravity wave which propagates on an interface between two fluids of different density. In the atmosphere, a bore typically develops when a gravity current enters a stably stratified boundary layer. Physics of bores depend on the depth of the stable layer, depth of the gravity current, stratification, and wind in the atmosphere above the inversion. Depending on the Brunt-Vaisala frequency, wind shear, and phase speed, vertically propagating gravity waves can be trapped leading to multiple reflections from the upper layers and wave-train appearance or, alternatively, can become a solitary wave traveling ahead of or behind the initial disturbance. We are particularly interested in the entrainment process associated with the bore wave-train and the extent to which different PBL parameterization schemes can successfully reproduce the observed surface drying and warming (from mesonet and S-POL refractivity change computations) and the moistening and cooling aloft (from AERI and research aircraft data) associated with the bore passage.

In the early hours of June 4 2002, a slowly moving cold front was positioned across the Oklahoma Panhandle as seen in temperature/dewpoint change and wind shift at mesonet stations (Fig. 1). Behind the front, a series of rain producing thunderstorms and at later times multiple linear structures which we associate with a bore can be seen in S-POL reflectivity (Fig. 2). Existence of the bore is further confirmed by FM-CW radar profiles at Homestead and ISS pressure, temperature and relative humidity traces showing passage of the second bore at 1040 UTC (Fig. 3).

Based on these circumstances, we believe that the bore originated when an outflow induced by the precipitation from a thunderstorm approached and strengthened the cold front, which pushed into a stable boundary layer ahead of the front.

3. NUMERICAL MODELING

Simulations with MM5 were performed to model the bore event. Initial and lateral boundary conditions were provided by the 20 km resolution hourly analysis produced by the Rapid Update Cycle (RUC) 3DVAR. Four one-way computational domains which have resolutions of 18, 6, 2 and 0.666 km, are shown in Fig 4. The domains had 32 vertically stretched levels except in the highest resolution domain where 44 vertical levels were used with the lowest model level at 10 m. All grids were initialized at 0000 UTC 4 June 2002. Grell-Devenyi (2002) ensemble based convective scheme was used in the two lower resolution domains. Reisner (1998) parameterization of resolved precipitation, Burk-Thompson (1989) implementation of 1.5-order Mellor-Yamada (1982) closure, Smirnova et al.'s (2000) soil model and RRTM radiative scheme (Mlawer et al. 1997) were used in the control simulation. Results of the 2 km simulation provided lateral and boundary conditions for the 0.666 km domain runs in sensitivity studies with respect to different turbulence parameterizations.

Accumulated 1 hour precipitation and surface temperature and wind are shown over domain 2 in Fig. 5. Comparison with Fig. 1 shows that the front's position was well reproduced. Comparison with Fig. 2 shows that thunderstorms in the simulation over Colorado occurred too early by about two hours, but the storms over western Kansas were not forecast to occur. In Fig. 6 surface wind divergence and air temperature are shown (domain 3). It can be seen that precipitation in southern Colorado caused a series of southeast propagating outflows similar to those seen in the analysis in Fig. 2. As seen in Fig. 7 (domain 4), where cross-front wind in the frame of reference moving with the front is shown, an outflow from the thunderstorms apparently steepened and strengthened the front which displayed a shallow elevated head, not unlike a gravity current. Interaction of this shallow cold front with the stable boundary layer ahead induced a bore.

Origin of the wave-train visible at the later time appears to be a result of multiple reflections of vertically propagating gravity waves from the upper layers of the atmosphere associated with Scorer parameter

$$S = \frac{N^2}{(u-c)^2} - \frac{1}{(u-c)}\frac{\partial^2 u}{\partial z^2},$$

where N is Brunt-Vaisala frequency, u is wind speed, and c is wave phase velocity. Mechanism of wave trapping and reflection was explained by Holton (1992, pp. 283-284) and exemplified for bores by Crook (1988). Since the waves have similar amplitude and propagate with the same phase velocity, the wave-train is not a result of a dispersion as suggested by Mahapatra et al. (1991). Its origin is also different from bores observed in a water tank by Simpson (1987, pp 188-191) where subsequent humps were formed when a gravity current head rebuilt itself after the first impact with the lighter fluid and, not unlike an oscillator, repeatedly impinged on the lighter fluid.

4. SENSITIVITY STUDIES AND TURBULENCE

Additional numerical experiments were conducted to reveal the sensitivity of the simulated bore propagation to various vertical turbulent mixing schemes that result from different implementations of the Mellor-Yamada 1.5-order turbulence model. In addition to the Burk-Thompson (BT) scheme, the original ETA scheme (Janjic 1994) and the modified ETA scheme (QL) were used in the experiments. The BT and ETA schemes differ in the treatment of the surface layer, the numerical technique to solve the turbulent kinetic energy equation (TKE, denoted as $q^2/2$) equation, and the realizability constraints on the diagnosed master length scale (l). The difference between the QL and the ETA schemes is that to obtain the master length scale (l), the former solves a prognostic equation for $q^2 l$ that is analogous to the TKE equation (Mellor and Yamada 1982) but involves a different set of closure constants:

$$\frac{\partial}{\partial t}\left(q^2 l\right) - \frac{\partial}{\partial z}\left[qlS_l \frac{\partial}{\partial z}\left(q^2 l\right)\right] = P_{sl} + P_{sl} - \varepsilon_l$$

where q^2 is twice the TKE, l is the master length scale,

$$P_{sl} = lE_1 P_s,\ P_{bl} = lE_2 P_b,\ \varepsilon_l = E_3 \frac{q^3}{B_1 l}\left[1 + E_4\left(\frac{l}{\kappa L}\right)^2\right],$$

Ps and P_b are shear and buoyancy TKE production terms, S_l, E_1, E_2, E_3 and E_4 are the closure constants, κ is the von Kármán constant and L is the vertical distance from the bottom surface. In the QL scheme, the same numerical technique as used in the ETA scheme is applied to solve both prognostic equations for TKE and the master length scale.

In Fig. 8 a snapshot of TKE using the three schemes is shown. It can be seen that despite significant differences in the magnitude of TKE, characteristics of the bore such as phase speed, amplitude, and number of waves (3) are quite similar in all the simulations. Only a slight difference exists for the QL scheme manifesting itself in a smaller wave amplitude. It should be added that other simulations with the QL scheme were also performed varying values of parameters in the mixing length equation, but these had little effect on the bore appearance. Apparent lack of sensitivity of the bore to the three turbulence parameterization and adequateness of one dimensional turbulence parameterization will be examined further in LES simulations with ARPS with the hope to present them

at the conference.

5. ENTRAINMENT AND BOUNDARY LAYER GROWTH

Boundary layer growth occurs through mixing of the air from the free atmosphere (entrainment) and lifting of the mixed layer and can be expressed as

$$\frac{\partial h}{\partial t} = E + W_h \quad ,$$

where h is mixed layer height, $E = -\left(\overline{w's'}\right)_h \Big/ \Delta s$ is entrainment velocity, Δs is a jump of a scalar value across the inversion and h is vertical velocity at h.

With vertical velocities of the order of 2 m s^{-1}, boundary layer growth in the initial stage of the bore is almost entirely due to the uplifting of the pre-frontal air. Generation of turbulence and entrainment in the wake of the bore can be attributed to strong shear induced initially by a gradient in along-front wind and later by gravity waves (Figs. 9 and 10). One-dimensionality of the BT scheme might limit its applicability in such circumstances. Current simulations with the full TKE equation using ARPS should alleviate this problem and provide guidance on general limitations of 1.5-order schemes in such applications.

5. REFERENCES

Burk, S.D., W.T. Thompson, 1989: A vertically nested regional numerical weather prediction model with second-order closure physics, *Mon. Wea. Rev.*, **117**, 2305-2324.

Crook, N.A., 1988: Trapping of low-level internal gravity waves, *J. Atmos. Sci.*, **45**, 1533-1541.

Grell, G.A., and D. Devenyi, 2002: A generalized approach to parameterizing convection combining ensemble data and data assimilation techniques, *Geophys. Res. Letters*, **29**, 10.1029/2002GL015311.

Holton, J.R., 1992: An introduction to dynamic meteorology, Academic Press, Inc., 512 pp.

Janjic, Z.I., 1994: The step-mountain eta coordinate model: Further developments of the convection, viscous layer, and turbulence closure schemes, *Mon. Wea. Rev.*, **122**, 927-945.

Mahapatra, P.R., R.J. Doviak, and D.S. Zrni, 1991: Multisensor observation of an atmospheric undular bore, *Bull. Amer. Meteor. Soc.*, **72**, 1468-1480.

Mellor, G.L., and T. Yamada, 1982:Development of turbulence closure model for geophysical fluid problems, *Rev. Geophys. Space Phys.*, **20**, 851-875.

Mlawer, E.J., S.J. Taubman, P.D. Brown, M.J.Iacono, and S.A. Clough, 1997: Radiative transfer for inhomogeneous atmospheres: RRTM, a validated correlated-k model for the longwave, *J. Geophys. Res.*, **102 (D14)**, 16,663-16,682

Reisner, J., R.J. Rasmussen, and R.T. Bruintjes, 1998: Explicit forecasting of supercooled liquid water in winter storms using the MM5 mesoscale model, *Quart. J. Roy. Meteor. Soc.*, **124**, 1071-1107.

Simpson, J.E., 1987: Gravity currents in the environment and the laboratory, Ellis Horwood Ltd., 244 pp.

Smirnova, T.G., J.M. Brown, S.G. Benjamin, and K. Dongsoo, 2000: Parameterization of cold-season processes in the MAPS land-surface scheme, J. *Geophys. Res.*, **105(D3)**, 4077-4086.

Xue, M., K.K. Droegemeier, V.Wong, A. Shapiro, and K. Brewster, 1995: *ARPS user's guide*. CAPS, University of Oklahoma, pp. 380.

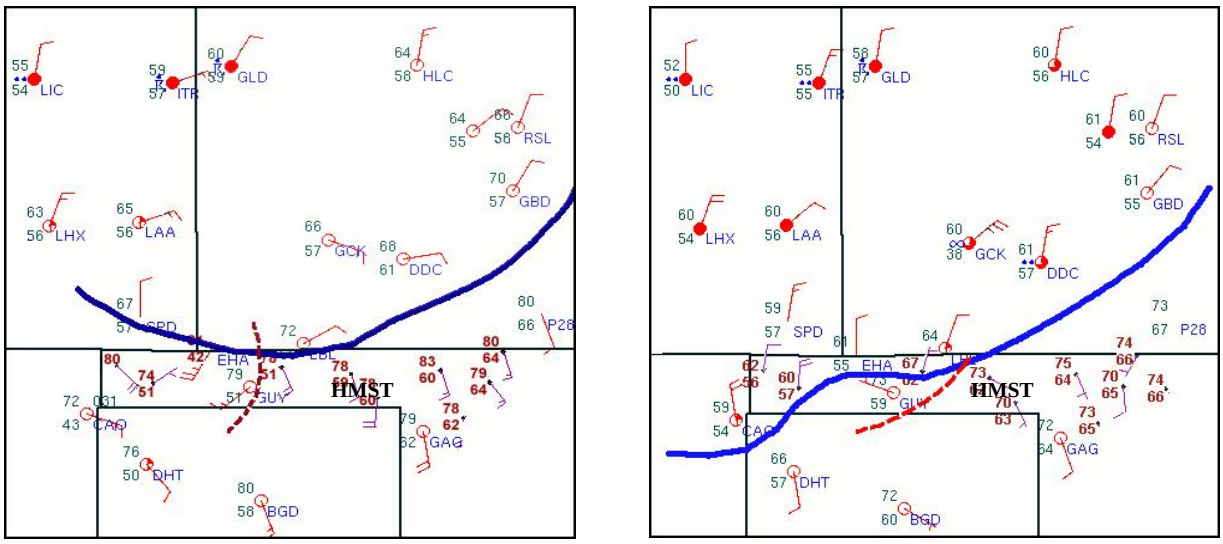

Figure 1. NWS surface stations reports at 0500 and 1000 UTC on 4 June 2002 with frontal analysis. Location of Homestead instrument array (HMST) marked. Solid lines are the locations of the cold front, and dashed lines are the locations of the bore A (left) and B (right).

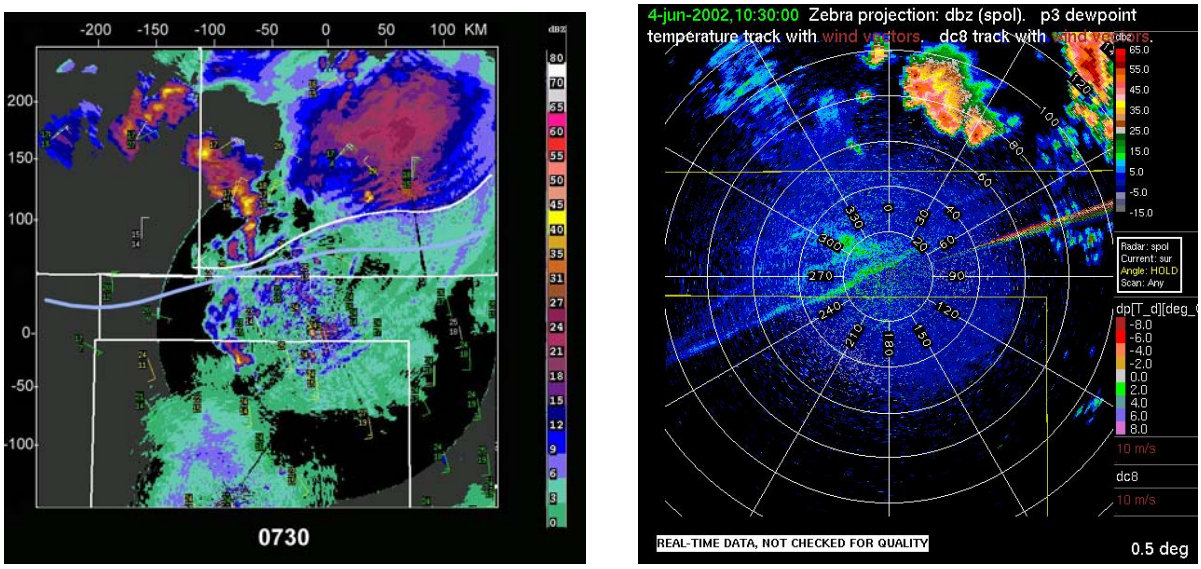

Figure 2. S-POL radar images at 0730 and 1030 UTC on 4 June 2002, blue line denotes the cold front, white line enotes thunderstorm outflow.

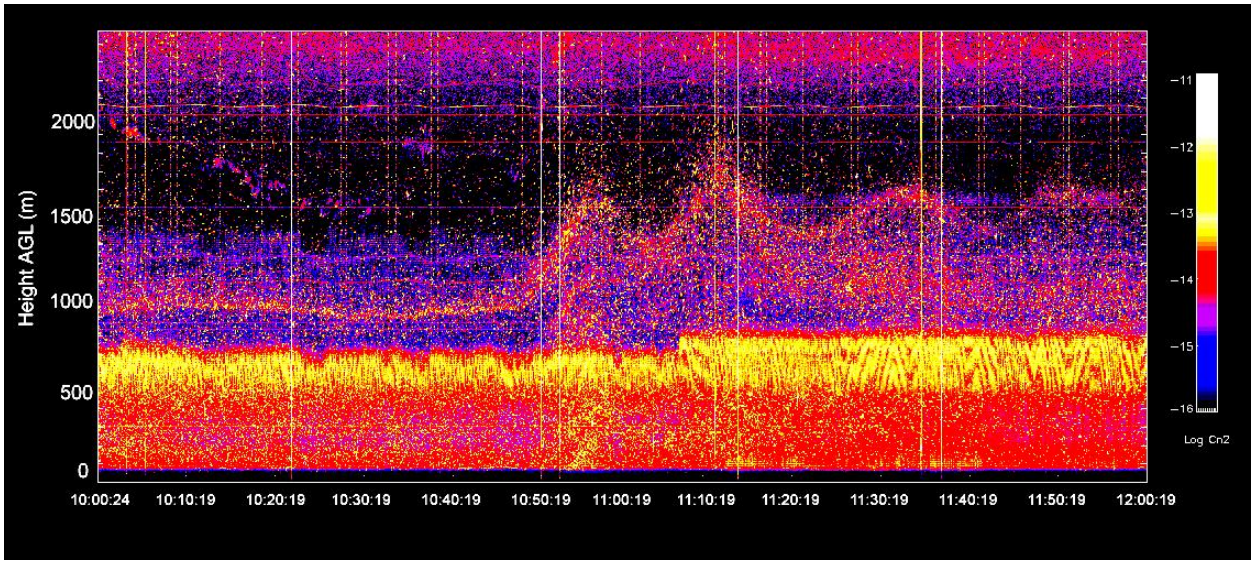

(a)

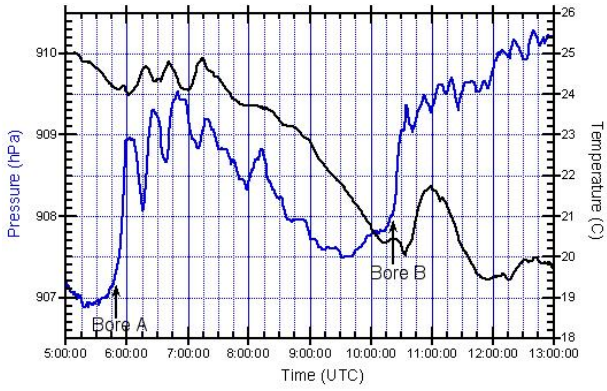

(b)

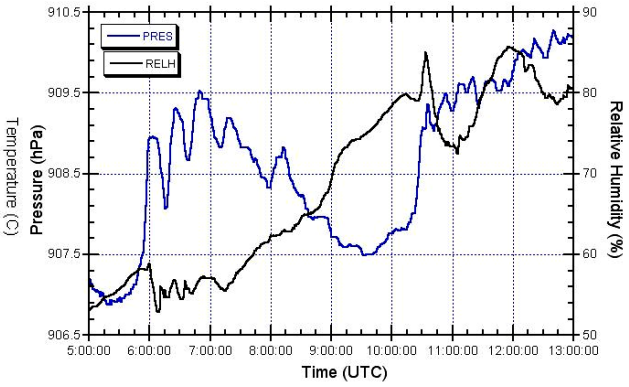

(c)

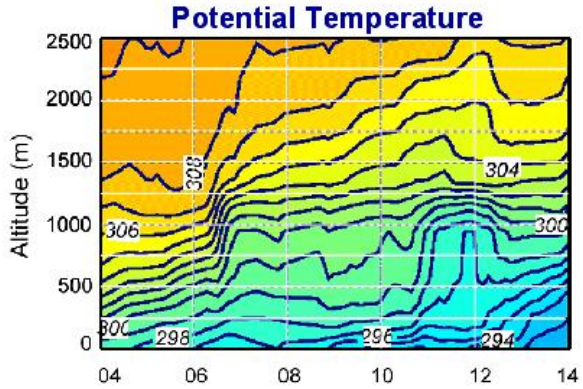

(d)

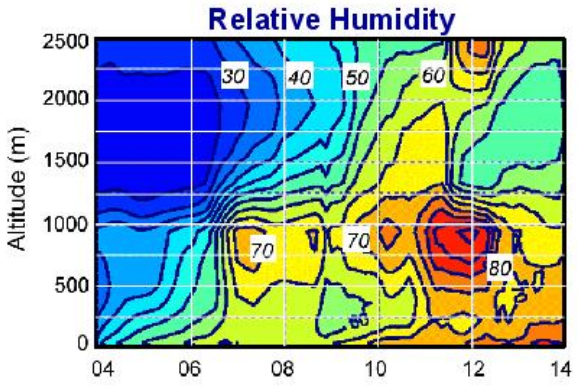

(e)

Figure 3. FC-MW radar showing the display of structure function (log C_n^2) at Homestead from 1000 to 1200 UTC 4 June 2002 (a), ISS surface pressure, temperature (b) and humidity (c) recorded at Playhouse, and AERI potential temperature (d) and relative humidity (e) from 0500 to 1300 UTC 4 June 2002 at Homestead.

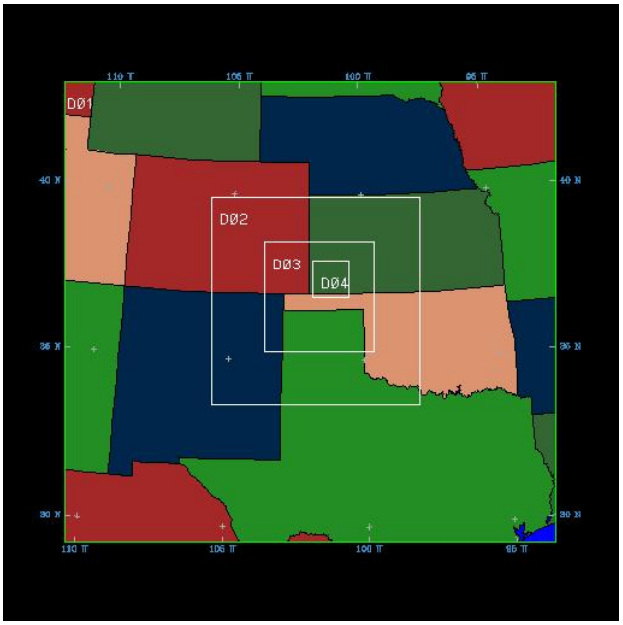

Figure 4. Modeling domains.

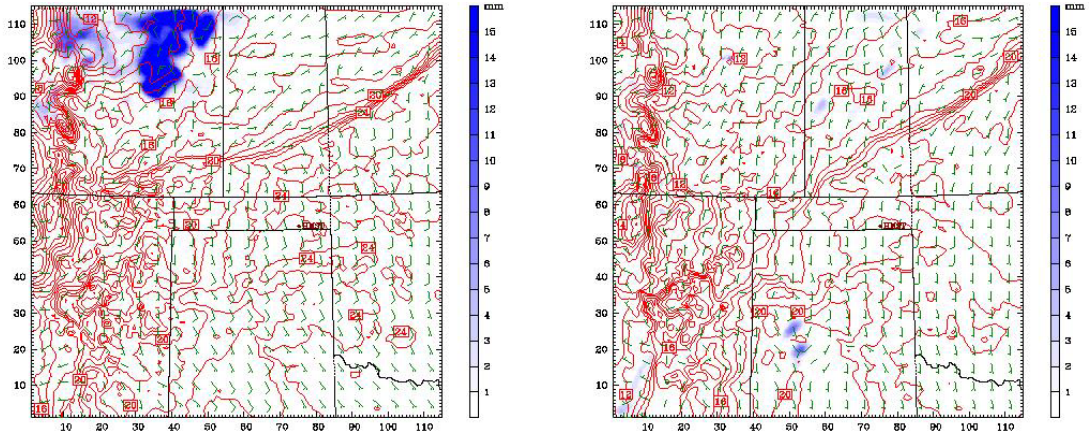

Figure 5. Hourly accumulated precipitation (mm), surface wind (full barb at 10 m s^{-1}) and temperature (°C) at 0500 (left) and 1000 (right) UTC on 4 June 2002 in the control simulation.

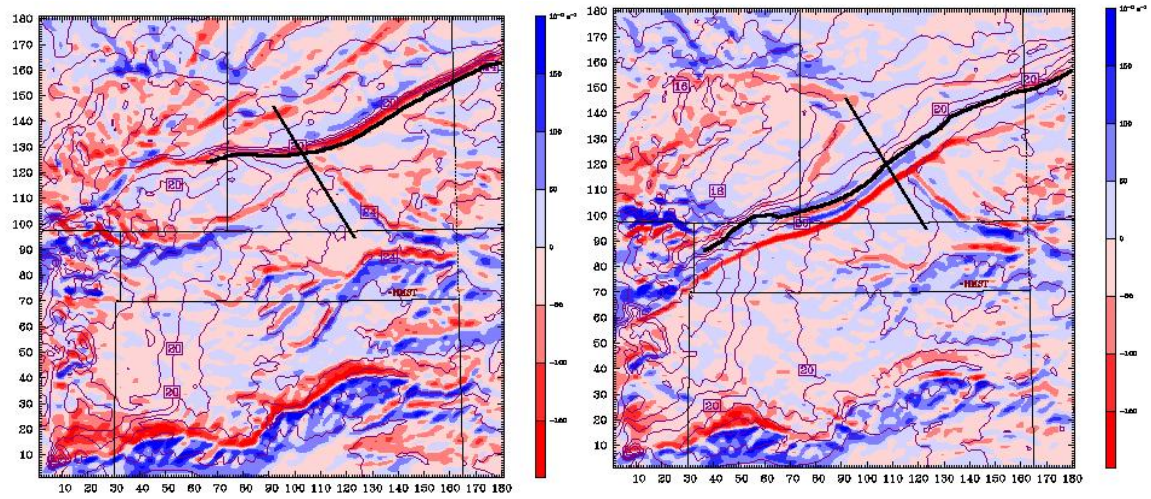

Figure 6. Surface divergence (10^{-5} s $^{-1}$, blue - divergent, red - convergent) and air temperature (°C) at 0600 (left) and 0845 (right) UTC on 4 June 2002 in the control simulation.

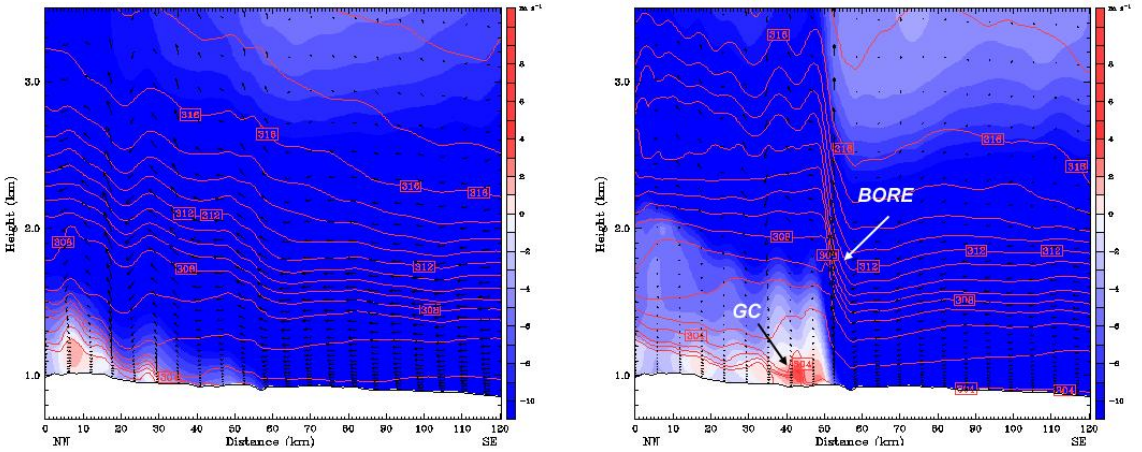

Figure 7. Cross-front relative wind (m s^{-1}) and isentropes of potential temperature (K) at 0700 (left) and 0800 (right) UTC on 4 June 2002 in the control simulation. Cross section is along the line in Fig. 6, and GC denotes the head of the gravity current.

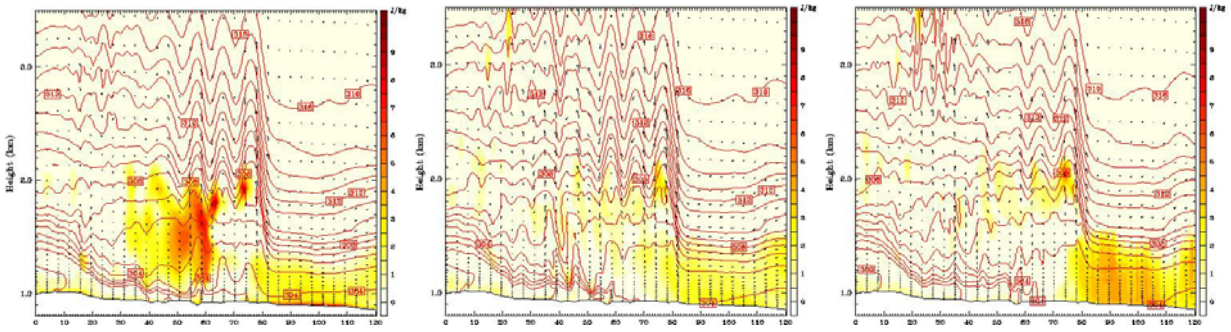

(a) (b) (c)

Figure 8. TKE (J kg $^{-1}$), isentropes of potential temperature (K) and circulation vectors at 0900 UTC 4 June 2002

for Burk-Thompson (a) , ETA (b) and QL (c) schemes.

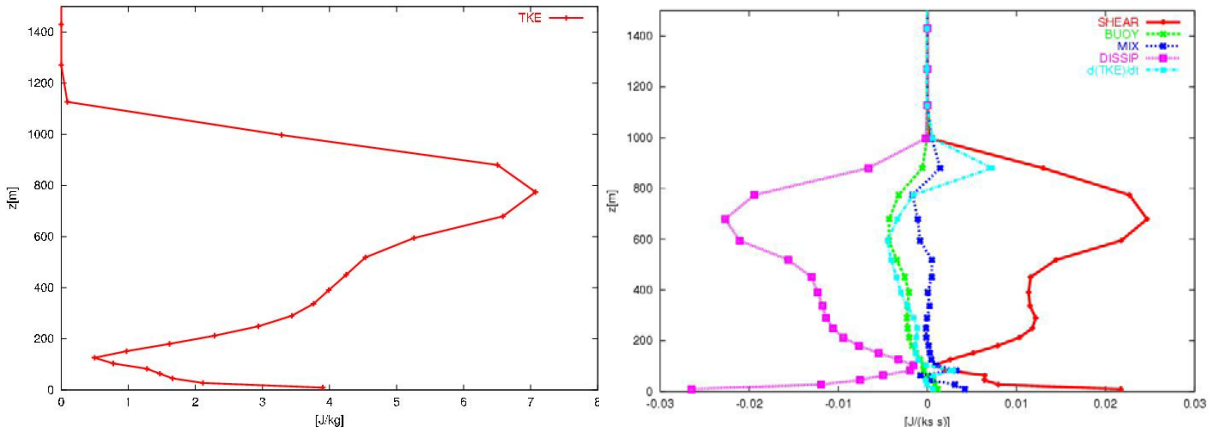

Figure 9. TKE (J kg $^{-1}$, left) and TKE budget (right) taken at middle point of cross-section at 0900 UTC on 4 June 2002 for BT scheme.

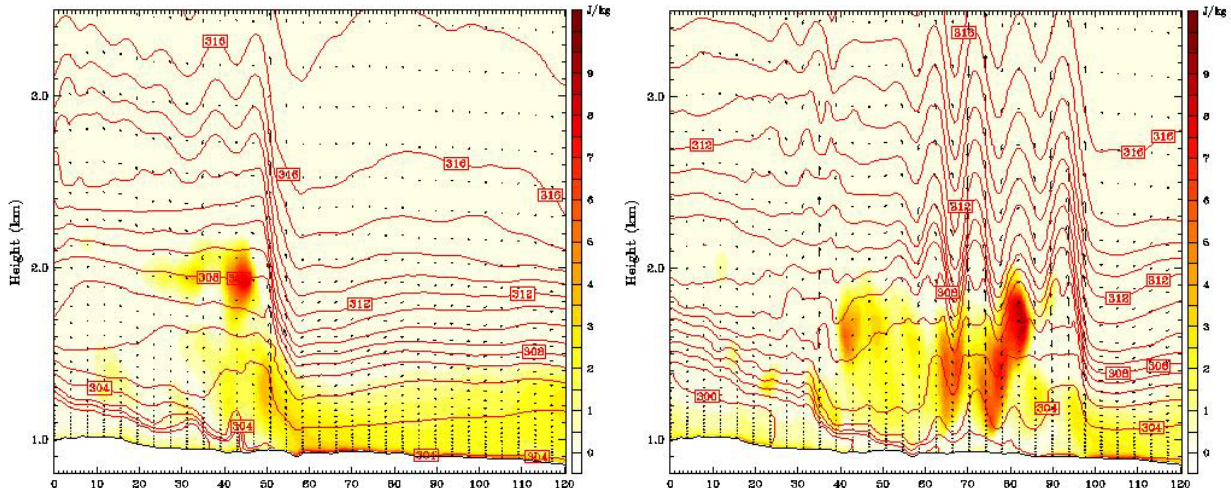

Figure 10. TKE (J kg $^{-1}$), isentropes of potential temperature (K) and circulation vectors at 0800 (left) and 0930 (right) UTC on 4 June 2002 for BT scheme.